Journal of Materials and Electronic Devices 1 (2025) 12-20

Three-Dimensional Design of a Robotic Hand with Proximal and Distal Interphalangeal Joints

Leyla ARSLAN[1], Muhammet AYDIN[2,*]

[1]Firat University, Faculty of Engineering, Department of Mechatronics Engineering, Elazig, Turkiye
[2]Firat University, Faculty of Engineering, Department of Mechatronics Engineering, Elazig, Turkiye

The human hand, with its intricate joint architecture and high dexterity, is one of the most compelling exemplars of biomechanical systems. In recent years, biomimetic approaches in robotic hand design have gained prominence, aiming to reproduce human-like motion for industrial manipulation, prosthetics, and rehabilitation. However, many existing studies model the metacarpophalangeal (MCP) joints while giving insufficient attention to the proximal interphalangeal (PIP) and distal interphalangeal (DIP) joints. In this study, inspired by the biomechanics of the human hand, it is presented a three-dimensional robotic hand that explicitly incorporates the PIP and DIP joints. Using SolidWorks, It has been modelled finger joints, phalangeal structures, and motion constraints in detail. The resulting model more faithfully reproduces physiological ranges of motion, yielding a representation that is closer to natural hand kinematics. This work provides a foundation for subsequent development of control algorithms and physical prototyping, and underscores the importance of biomimetic design in robotic hands.

Keywords: *Robotic hand, Biomimetic design, Interphalangeal joints, Three-dimensional modelling*

Submission Date: *01 June 2025*
Acceptance Date: *20 August 2025*

**Corresponding author:* muhammeta@firat.edu.tr

1. Introduction

The human hand—characterized by its multi-joint architecture, high degrees of freedom, and fine motor skills—is one of the most intricate and inspiring examples in biomechanics. From daily tasks to industrial production, manual functionality plays a critical role. Accordingly, robotic research has moved beyond simple grasping to emphasize designs that replicate the hand's natural joint kinematics. Yet in much of the literature, metacarpophalangeal (MCP) joints are prioritized, while proximal interphalangeal (PIP) and distal interphalangeal (DIP) joints are often treated as secondary; this limits overall dexterity and motion fidelity compared to the human hand.

This study addresses that limitation by presenting the three-dimensional design and simulation of a biomimetic robotic hand that explicitly includes the PIP and DIP joints. The model was developed in SolidWorks; phalanx and joint geometries were constructed with anatomical references, assembly (mate) constraints and range-of-motion limits were defined, and each joint was driven by an independent servo motor to realize a fully actuated architecture. This enables independent finger motion while targeting human-like, realistic kinematics.

Throughout the modeling process, material assignments, assembly tolerances, servo layouts, and naming conventions have been treated systematically. Representative motion scenarios and joint ranges have been validated using SolidWorks Motion Study, aligning manufacturability (tolerance and packaging) with control-oriented needs (independent actuation and angle limits).

The present work is limited to digital modeling and simulation; physical prototyping is outside the current scope. In this form, the design provides a practical foundation for subsequent development of control algorithms, hardware selection, and prototyping efforts.

1.1. History and development process of robotic hand systems

Early work on robotic hands focused on highly articulated, multi–degree-of-freedom (DoF) designs that emulate the human hand. Driven by biomimicry, these prototypes sought to replicate human joint kinematics as faithfully as possible, which in turn required numerous joints and actuators and yielded mechanically complex structures. The resulting complexity—together with high manufacturing and maintenance costs and the difficulty of deploying control algorithms—limited their practical use [1]. From the 2000s onward, attention shifted to underactuated designs that reduce mechanical burden. Notably, the iHY project demonstrated robust, low-cost hands capable of a diverse range of grasps with only five actuators [2]. More recently, the field has moved toward integrating biomimetic design with AI-based learning and tactile feedback, producing multi-finger manipulation that is more natural, adaptable, and human-like. This trajectory draws on the neural control principles of the biological hand while enhancing adaptive grasping and environmental compliance in robotic applications [3].

1.2. Human hand anatomy and robotic compatibility

In the human hand, the metacarpophalangeal (MCP) joints are condylar (ellipsoid) structures with two degrees of freedom, whereas the proximal interphalangeal (PIP) and distal interphalangeal (DIP) joints are single–degree-of-freedom hinge joints [4]. Accurately modeling these distinct joint types in robotic systems is essential for achieving realistic hand motions. In particular, many robotic designs neglect the PIP and DIP joints, which restricts dexterity and makes it difficult to attain human-like performance targets [5].

1.3. Biomechanical models and adaptation to robotic systems

Coordination of finger movements is governed by the kinematic couplings of the tendon–muscle system, especially the relationship between the PIP and DIP joints. Studies have shown that PIP extension can elicit motion at the DIP joint [6]. In biomimetic robotic systems, tendon routing, joint range-of-motion limits, and moment arms should be designed in a manner consistent with these native couplings. Advanced biomechanical modeling tools now enable detailed digitization of the hand's musculoskeletal architecture. Notably, the comprehensive AnyBody™ hand model developed by Engelhardt et al. (2020) represents anatomical muscle paths, joint limits, and the muscle–tendon architecture with high fidelity, providing a valuable biomechanical reference for robotic design [7].

1.4. Normative findings on the joint structure of the human hand

Range-of-motion (ROM) data for the human hand provide reliable reference points for robotic finger modeling. In an observational study of Indian individuals, active ROM values for the finger joints were reported as follows:
Index finger:

- PIP flexion: mean 97.2 ± 16.9°
- DIP flexion: mean 81.6 ± 13.9°
- MCP flexion: mean 86.0 ± 9.2°

Values for the other digits were of comparable, though not identical, magnitude; notably, DIP flexion tended to be slightly greater in the little finger. These normative measurements are highly useful for CAD modeling, defining joint limits, and developing realistic control strategies in robotic hand design [8].

1.5. Overview of material and actuator selection in robotic hand systems

Actuator and material choices in robotic hand design are critical determinants of system performance, energy efficiency, and the intended application domain. The most widely used actuators in the literature include servo motors, DC motors, and tendon-driven mechanisms. These platforms enable independent joint control and precise positioning; however, increases in motor count, mass, and cable-routing complexity impose significant constraints—particularly in high–degree-of-freedom (DoF) designs [9].
As alternatives, recent years have seen the rise of pneumatic artificial muscles (PAMs) and soft-material-based actuators. These devices attract attention due to their biomimetic similarity to the human muscle–tendon system, structural compliance that supports safe human–robot interaction, and high power-to-weight ratios [10]. Collectively, they offer a promising route to overcoming the mechanical limitations of conventional motor–tendon systems.
From a materials perspective, aluminum alloys and 3D-printed polymers (e.g., PA12, PLA, ABS) are prominent for rigid components, whereas silicone elastomers, TPU, and hydrogels stand out for compliant structures. These materials provide advantages for achieving biomimetic motion, shortening prototyping timelines, and optimizing costs. Nevertheless, because this study focuses exclusively on three-dimensional modeling in a digital environment, material and actuator selection lies outside the present scope. For future prototyping, it is recommended to consider the high positional precision of servo-motor–tendon mechanisms, the biomimetic compliance of silicone-based

elastomers, and the rapid manufacturability afforded by 3D-printed polymers [11].

1.6. Literature review on robotic hand designs

The prevailing trend in anthropomorphic finger design is to re-establish the human hand's native PIP–DIP coupling through mechanical means. Linkage-driven approaches—particularly crossed four-bar kinematics—can produce the single-DoF flexion at the PIP while coupling the DIP in a controlled manner, thereby keeping part count and packaging within manageable bounds [12]. Although earlier studies emphasized the strong coupling between PIP and DIP flexion, more recent research has shown that high–degree-of-freedom (DoF) prosthetic hands can approach human-level functionality. In particular, the lightweight 19-DoF prosthesis developed by Yang et al. (2025) achieves substantial grasp diversity and near-human functional performance, contributing to biomimetic fidelity [13].

Within the tendon-driven design line, task-based grasp analysis informs route/anchor planning that systematically determines tendon paths and moment arms [14]. A recent quantitative survey statistically mapped relationships between design variables (DoF, actuation type, primary transmission architecture) and performance metrics (speed, mass, fingertip force, compactness), reporting that underactuated grasps frequently leverage PIP–DIP coupling for natural grasping, whereas fully actuated designs increase motion diversity at the expense of complexity and volume [15]. These findings provide design-scale guidance during the CAD phase (e.g., SolidWorks) on when joint coupling should be favored under specific task scenarios [14-15].

Biomechanical evidence is crucial for anthropomorphic validation of PIP–DIP kinematics. A cadaveric study disentangled intrinsic–extrinsic contributions within the PIP extension mechanism, clarifying the basis of PIP/DIP motion coupling; such results quantitatively ground design decisions on joint limits and on passive versus active coupling [16]. Likewise, detailed musculoskeletal hand models (the AnyBody-based detailed hand model and a comprehensive open-source wrist–hand model) offer reliable reference sets for CAD dimensioning—alignment of joint axes, assignment of ROM bounds, and selection of phalangeal segment proportions [17-18].

From the standpoint of feasible and manufacturable linkage architectures, the open-source HRI Hand is instructive: using two underactuated four-bar finger mechanisms, it combines pre-shaping capability with low cost and compact packaging. Such exemplars make clear how mechanism topology (e.g., two serial four-bars) affects finger profile height, assembly, and cable routing; even absent prototyping, they inform appropriate geometric constraints at the CAD stage [19].

In sum, design-oriented literature addresses PIP–DIP coupling through several viable schemes (crossed four-bar, rod-linked four-bar, tendon-mediated coupling). While preserving (when needed) the separation of flexion and ab/adduction at the MCP, controlled PIP–DIP coupling yields advantages in packaging, mass, and layout [12, 14, 15]. Moreover, recent work indicates that high-DoF prosthetic hands support human-like functionality and anthropomorphic fidelity, reinforcing CAD-driven design choices [13]. When combined with anatomically aligned joint axes, ROM constraints, and properly proportioned phalangeal segments—as in the present study—this framework strengthens anthropomorphic fidelity at the design stage, independent of subsequent control and prototyping phases.

2. Material and Methods

2.1. General design structure

The human hand, from a biomechanical perspective, is a complex and functional structure composed of different types of joints. Thanks to these joints, the fingers attain a wide range of motion, making functions such as grasping, holding, and precise manipulation possible. In robotic hand designs, the aim is to create a model with high biomimetic fidelity by imitating the natural movements of these joints.

There are three fundamental joints in the fingers:

Metacarpophalangeal (MCP) joints: These condyloid joints, in addition to flexion–extension (bending–straightening), also allow abduction–adduction (moving away from and toward the hand's midline). In the human hand, MCP joints have approximately two degrees of freedom.

Proximal interphalangeal (PIP) joints: These are hinge-type joints that allow only flexion and extension. They have a single degree of freedom.

Distal interphalangeal (DIP) joints: Similar to the PIP joints, these are hinge-type joints that perform flexion and extension with a single degree of freedom.

The thumb, however, has a joint structure different from the other fingers. The thumb has a metacarpophalangeal (MCP) joint and an interphalangeal (IP) joint. Although the MCP joint can exhibit partially multi-axial motion, it is generally modeled as a single–degree-of-freedom hinge. The IP joint is a single-DoF hinge that performs flexion–extension.

Accurately modeling these joint types in robotic designs increases both the naturalness of finger movements and the reliability of grasp tasks. As shown in Figure 2.1, correctly modeling the positions of the MCP, PIP, and DIP joints as in the human hand is of critical importance, especially for precise manipulation and human-like grasping capability.

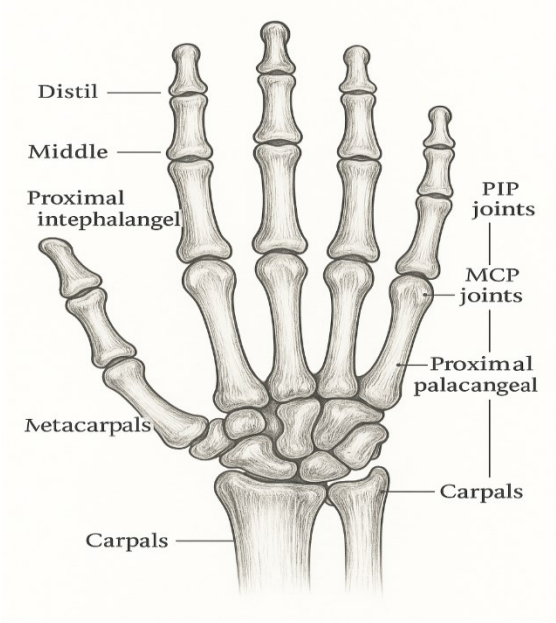

Fig.1. Schematic representation of the human hand's MCP, PIP, DIP, and thumb IP joints

2.2. Pre-actuation baseline design

A 3D CAD model shown in Figure 2 without actuators was constructed on the basis of the human hand's joint architecture. The objective is to represent anthropomorphic kinematics with fidelity and to define a precise geometric framework for packaging, mounting surfaces, and transmission routes. Material assignment and structural/thermal analyses are outside the scope of this stage.

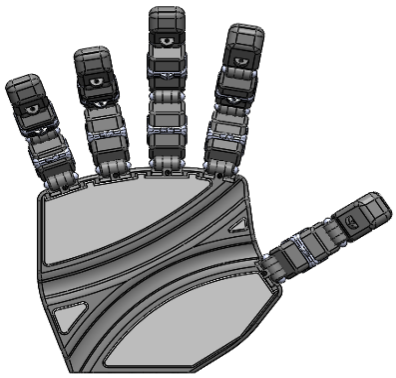

Fig.2. Actuation-free baseline CAD model (full-hand view) showing finger segments and palm packaging

The kinematic architecture adopts three phalanges per finger connected in series, with joints represented to reproduce native motions. The metacarpophalangeal (MCP) joint is modeled with two degrees of freedom—flexion–extension and abduction–adduction about orthogonal axes. The proximal (PIP) and distal (DIP) interphalangeal joints are treated as single-DoF hinges; a fixed-ratio mechanical coupling is implemented such that DIP motion is functionally dependent on PIP flexion, as illustrated in Figure 3. In the thumb, the MCP and interphalangeal (IP) joints are represented as single-DoF hinges.

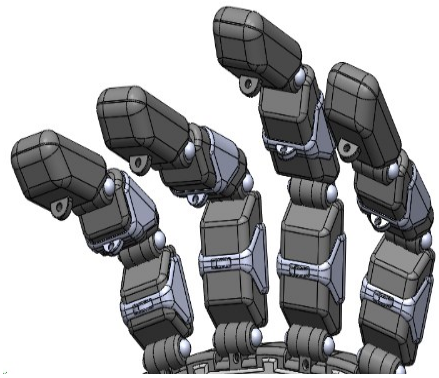

Fig.3. Detail view of the fingers highlighting the MCP, PIP, and DIP regions and the linkage-based coupling

Geometric sizing and constraints focus on preserving anthropomorphic proportions. Phalanx lengths, joint centers, and joint-axis directions are positioned in parallel with anatomical alignments, and each joint's range of motion is assigned in the CAD environment via LimitAngle constraints. This prevents hyperflexion and geometric interference, eliminating self-contact risk along fingertip trajectories. The palm geometry is shaped to provide packaging compatibility with the finger base joints, and clear routes for cabling/tendons are defined. Reserved volumes and anchoring surfaces for future actuators and transmissions are specified unambiguously.

The CAD implementation follows a top-down workflow. Skeleton sketches establish joint centers and segment lengths; phalanges, linkage elements, and joint blocks are modeled parametrically. During assembly, revolute joint/axis mates and limit-angle constraints are applied, and mechanism closure is verified across the full motion range. Interference and degrees-of-freedom analyses ensure that the four-bar coupling arrangements remain solvable in all configurations and that packaging integrity is preserved within the finger profile.

Validity conditions are explicit: all components are treated as rigid, and joints are ideal revolute pairs; friction, backlash, and elasticity are not included at this stage. These assumptions are specific to a design phase that prioritizes kinematic fidelity.

2.3. Biomimetic references and anthropometric criteria

In this study, “similarity to the human hand” was pursued along three axes: (i) dimensional scaling, (ii) anatomical alignment of joint axes, and (iii) joint motion relationships and limits.

2.3.1. Dimensional scaling

The design was referenced to the nominal dimensions extracted from the provided technical drawing (overall length ≈ 284.6 mm, plan-view lateral span ≈ 226.6 mm) and uniformly scaled to match adult hand anthropometry. The practical target corresponds to glove sizes 9–10 (L–XL), yielding a hand length of ≈192–204 mm. The relative length ordering among digits (middle > ring/index > little) and the ratio of total thumb length to the middle finger were preserved.

2.3.2.Joint centers and axis alignment

For each finger, the MCP–PIP–DIP rotational axes were defined as mutually parallel within the local sagittal plane, and revolute definitions were placed at condylar centers in the phalanx models. During assembly, translational and angular misalignments were minimized to prevent axis drift during finger motion. The finger splay angles and the thumb offset documented in the drawing were retained to maintain a natural placement within the palm.

2.3.3.Motion relationships and limits

Synchronous PIP–DIP flexion was implemented via a biomimetic kinematic coupling, preserving the natural dependence of the DIP on the PIP (target coupling coefficient k ≈ 0.6–0.7). Joint motions were constrained with LimitAngle features to realistic ranges: MCP 0–90°, PIP 0–100°, DIP 0–80°, thumb MCP 0–60°, thumb IP 0–80°. These limits were selected to avoid contact/interference during full opening–closing while maintaining fingertip stability during grasping.

The model was uniformly scaled from the nominal dimensions in the provided technical drawing to the L–XL anthropometric range representative of average adult hands; because the dimension/scale relationships were defined parametrically in SolidWorks, the prototype size can be readily adjusted as needed while preserving proportions. The joint axes were aligned to anatomical references, and the PIP–DIP kinematic coupling together with the range-of-motion (ROM) limits were set within intervals consistent with human hand data reported in the literature; these choices aim to achieve human-like ergonomics and support biomimetic adequacy in the CAD assembly and motion analysis.

2.4. Motor selection criteria

Three primary criteria govern the choice of motors for the robotic hand:

Torque: Must be sufficient to generate the fingertip forces required during grasping and object holding. Insufficient torque can lead to failure to secure objects or to reduced simulation fidelity.

Size (Envelope): Compact form factor is critical for integration within the palm housing and finger mechanisms. Oversized motors can compromise the hand’s biomimetic geometry; therefore, small-form-factor servo motors are preferred.

Speed (Angular Velocity): To achieve human-like response times, motors should operate above a minimum angular-speed threshold. Very slow motors constrain manipulation capability, whereas excessively fast motors can challenge control stability.

2.5. Specifications and suitability of the selected motor

In this study, the MG90S micro servo motor was chosen. With its compact dimensions (22.8 × 12.2 × 28.5 mm), low mass (~13 g), and metal gear train, the MG90S delivers high durability within a small envelope. Its technical specifications are provided in Table 1 [20].

Tablo 1. Technical specifications of the MG90S micro servo motor [20]

Feature	Value
Operating voltage	4.8 – 6.0 V
Torque capacity	2.2 kg·cm (4.8 V), 2.5 kg·cm (6 V)
Speed	0.10–0.12 s / 60°
Max rotation angle	~180°
Dimensions	22.8 × 12.2 × 28.5 mm
Mass	~13 g
Gear train	Metal

The characteristics of the MG90S motors both provide the torque required at the finger joints and, thanks to their compact form factor, allow integration into the hand without compromising biomimetic proportions. In addition, their response speed and built-in position feedback make them well suited for PID-based control.

2.6. Number and arrangement of motors

To enhance biomimetic dexterity and enable independent control at each joint, a dedicated servo motor is assigned to every phalangeal joint. This approach transfers the native joint behavior of the human hand more faithfully into the digital model and establishes a suitable multi-input–multi-output (MIMO**)** control architecture.

The joint–motor distribution across the fingers is organized as follows:

• Four fingers (index, middle, ring, little): Each uses 3 independent servo motors for the MCP, PIP, and DIP joints (4 fingers × 3 joints = 12 servo motors).

• Thumb**:** By anatomy, the thumb comprises the MCP and IP joints; therefore, 2 independent servo motors are assigned to the thumb (1 thumb × 2 joints = 2 servo motors).

Each motor is mounted directly at its corresponding joint and positioned along the phalangeal segments in close proximity to the joint centers. This placement enables fully independent finger motions and makes the hand's natural kinematics more transparent in simulation. By distributing the actuators on a joint-by-joint basis, the design departs from the underactuated paradigm and adopts a fully actuated architecture, thereby allowing the fingers to perform coordinated tasks without being constrained to synchronized motion.

2.7. Servo motor placement and joint angle limits

2.7.1. Motor selection and layout

Each finger (index–middle–ring–little) is actuated at the MCP, PIP, and DIP joints, and the thumb at the MCP and IP joints, by independent micro servomotors. In the implementation, MG90S metal-geared micro servos were used. Independent actuation facilitates joint-level control and simplifies both kinematic analysis and control design. The mapping is as follows:

-Fingers (1–4): MCP → MG90S; PIP → MG90S; DIP → MG90S

-Thumb: MCP → MG90S; IP → MG90S

2.7.2. Kinematic transmission

The rotational motion at the servo shaft is converted (i) to linear push–pull via a crank–connecting-rod linkage, and (ii) back to rotational motion about the joint hinge axis. This two-stage transmission improves packaging and torque leverage while providing a biomimetic analogue to tendon–joint interaction.

2.7.3. Angle limits and ROM

Although the MG90S datasheet stroke is 0–180°, joint range of motion (ROM) was constrained in CAD via LimitAngle features to satisfy anthropometric targets and mechanical packaging:

- **MCP:** 0–90°
- **PIP:** 0–100°
- **DIP:** 0–80°
- **Thumb MCP:** 0–60°
- **Thumb IP:** 0–80°

2.7.4. Rationale

Directly coupling the servo output to the joint is suboptimal with respect to angle–travel scaling and risks of interference/stress. The linkage enables ergonomic motor placement, improved moment arm, and fine ROM tuning.

2.7.5. Verification

The ranges of motion (ROM) for the MCP, PIP, and DIP joints were specified based on the design's anthropometric and mechanical requirements; the LimitAngle constraints defined in the CAD environment, together with Motion Study outputs, indicate that these bounds are implemented in the model correctly and reproducibly. This approach helps ensure that the servo commands used in the control design remain within safe operating limits and are consistent with the targeted biomimetic ergonomics.

3. Results and Discussion

The CAD model of the robotic hand was created by modeling the finger phalanges and thumb components as independent parts and combining them via a hierarchical assembly referenced to the palm body. Finger sub-assemblies were placed sequentially; servomotors and linkage components were added in the final stage.

Mates and constraints. Revolute mates were assigned to the joint pins, and the single rotational degree of freedom was constrained with LimitAngle features (MCP 0–90°, PIP 0–100°, DIP 0–80°, thumb MCP 0–60°, thumb IP 0–80°). For positional placement, Coincident/Distance mates were used where required. To ensure smooth motion, 0.1–0.2 mm mechanical clearance was left in the assembly, while the clearance at the servo shaft–link interface was kept minimal.

Servo placement. Each joint is driven by an independent micro servo; servo shaft axes were arranged colinear with the corresponding joint rotation axes. Kinematic transmission is provided via a linkage mechanism.

This configuration prevents interference during assembly, yields joint kinematics close to that of the human hand, and enables reproducible range-of-motion (ROM) control; the overall assembly and servo placement are shown in Figure 4.

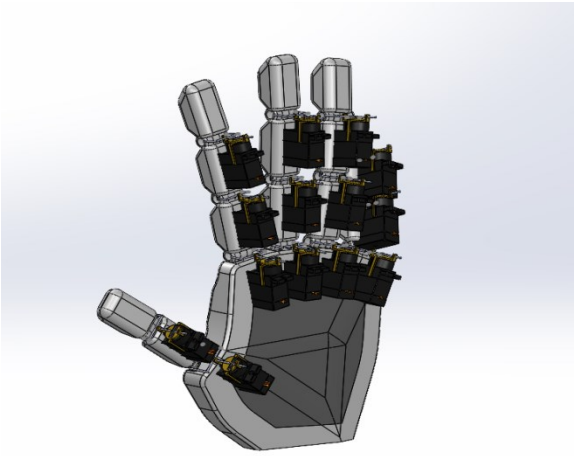

Fig.4. General assembly and servo placement

The motion simulations were conducted in SolidWorks Motion Study. The MCP–PIP–DIP joints and the thumb MCP–IP joint were exercised with rotational-motor inputs under the prescribed LimitAngle constraints. The analysis encompassed (i) finger-wise single cycles, (ii) a thumb cycle, and (iii) simultaneous closing–opening of all digits. The resulting angle–time profiles indicate that joint motions remained within the specified ROM bounds, that PIP–DIP synchrony was approximately linear over the operating range, and that no mechanical interference/penetration occurred. These findings verify the kinematic adequacy of the CAD model and confirm that the servo command trajectories used for control design remain within safe operating limits

In this study, Revolute mates were assigned to each finger joint (MCP–PIP–DIP) and thumb joint (MCP–IP) to enforce single-axis rotation, and the rotational degree of freedom was bounded with LimitAngle constraints. The rotation axes were aligned colinear with the corresponding servo shaft axes. The applied ROM intervals were defined as: MCP 0–90°, PIP 0–100°, DIP 0–80°, thumb MCP 0–60°, thumb IP 0–80°. This configuration models each joint as a stable single-DOF hinge and ensures that the prescribed LimitAngle values safely achieve the biomimetic range of motion targeted by the design.

Material selection prioritized a low mass–sufficient strength trade-off and ease of prototyping. Structural hand shells and phalanges were modeled in ABS to enable 3D printing with adequate impact resistance; motion-transmission members use Aluminum 1060 for stiffness and machinability; wear-prone pins/shafts use alloy steel for strength and abrasion resistance. Assigned materials in SolidWorks drive the mass properties calculations (mass, CoM, MOI). In Table 2, it has been given mass properties of the designed hand robot.

Tablo 2. Technical specifications of the MG90S micro servo motor

Component	**Material**	**Key property / Rationale**	**Recommended manufacturing**
Finger phalanges (P1–P3)	**ABS**	Lightweight, impact-resistant, tolerant to assembly; 3D-printable	FDM/SLA 3D printing
Servo housing	**ABS**	Protective shell for electronics; light and easy to shape	3D printing
Linkage arms	**Aluminum 1060**	High stiffness-to-weight; easily machinable; corrosion resistant	CNC milling/turning
Pins / shafts	**Alloy steel**	High strength; wear and friction resistance	Standard dowel/shaft or turned, with optional heat treatment/coating
Palm body	**ABS**	Main carrier; lightweight with structural continuity	3D printing
Thumb components	**ABS**	Geometric compatibility; fast prototyping; adequate toughness	3D printing

4. Conclusion

In this study, a three-dimensional model of a biomimetic robotic hand, inspired by the biomechanics of the human hand and explicitly incorporating the PIP and DIP joints, has been developed. While the literature typically focuses solely on MCP joints, leading to limited mobility in robotic hands, this model more realistically reflects the natural kinematics of the human hand. In the design carried out in the

SolidWorks environment, joint geometries, movement constraints, and servo motor arrangements were systematically modeled; simulation results showed that physiological movement ranges were successfully reproduced.

Although the study is limited to digital modeling and simulation, it provides a solid foundation for control algorithms, hardware selection, and physical prototype development. The results obtained demonstrate that biomimetic approaches play a critical role in increasing the functionality and grasping accuracy of robotic hands; they reveal that the design can contribute to both academic and industrial applications with experimental studies to be conducted in subsequent stages.

Acknowledgments

This study was produced from studies carried out within the scope of the first author's master's thesis topic.

References

[1] Piazza, C., Grioli, G., Catalano, M.G. and Bicchi, A., A century of robotic hands, Annual Review of Control, Robotics, and Autonomous Systems, 2:1 (2019) 1–32. https://doi.org/10.1146/annurev-control-060117-105003.

[2] Odhner, L.U., Jentoft, L.P., Claffee, M.R., Corson, N., Tenzer, Y., Ma, R.R., and Dollar, A.M., A compliant, underactuated hand for robust manipulation, The International Journal of Robotics Research, 33:5 (2014) 736–752. https://doi.org/10.1177/0278364913514466.

[3] Li, Y., Zhu, X., Wang, W., Guo, T. and Zhang, H., A survey of multifingered robotic manipulation: biological and robotic perspectives, Frontiers in Neurorobotics, 16 (2022) 843267. https://doi.org/10.3389/fnbot.2022.843267.

[4] Benson, D.C. and Varacallo, M., Anatomy, shoulder and upper limb, metacarpophalangeal (MCP) joints, StatPearls, StatPearls Publishing, (2023).

[5] Lu, S., Zhao, H. and Zhang, M., Finger multi-joint trajectory measurement and kinematics, Machines, 12:10 (2024) 1081. https://doi.org/10.3390/act13090332.

[6] Park, S.Y., Rhee, S.K., Kim, J.S., et al., Extension mechanism of the proximal interphalangeal joint of the human phalanx: a cadaveric biomechanical study, BioMed Research International, 2020 (2020) 2507239. https://doi.org/10.1155/2020/7585976.

[7] Engelhardt, L., Melzner, M., Havelkova, L., Fiala, P., Christen, P., Dendorfer, S. and Simon, U., A new musculoskeletal AnyBody™ detailed hand model, Computer Methods in Biomechanics and Biomedical Engineering, 24:7 (2020) 777–787. https://doi.org/10.1080/10255842.2020.1851367.

[8] BK, M.I., Baba, P.U.F., Singh, V., Karanjkar, A., Madhavan, L., Shah, R.A., and Krishnamoorthy, S., The normal active range of motion of the index, middle, ring, and little fingers in a sample of Indian population, Indian Journal of Plastic Surgery, 57:4 (2024) 248–255. https://doi.org/10.1055/s-0044-1788593.

[9] Odhner, L.U., Jentoft, L.P., Claffee, M.R., Corson, N., Tenzer, Y., Ma, R.R., Buehler, M., Kohout, R., Howe, R.D. and Dollar, A.M., A compliant, underactuated hand for robust manipulation, The International Journal of Robotics Research, 33:5 (2014) 736–752. https://doi.org/10.1177/0278364913514466.

[10] Kalita, B. and Dwivedy, S., A review on the development of pneumatic artificial muscle actuators: force model and application, Actuators, 11:10 (2022) 288. https://doi.org/10.3390/act11100288.

[11] Wang, Y., Wang, Y., Mushtaq, R. T., & Wei, Q., Advancements in soft robotics: A comprehensive review on actuation methods, materials, and applications, Polymers, 16:8 (2024) 1087. https://doi.org/10.3390/polym16081087.

[12] Kim, U., Jung, D., Jeong, H., Park, J., Jung, H.M., et al., Integrated linkage-driven dexterous anthropomorphic robotic hand, Nature Communications, 12 (2021) 7177. https://doi.org/10.1038/s41467-021-27261-0.

[13] Yang, H., et al., A lightweight prosthetic hand with 19-DOF dexterity and human-level functions, Nature Communications, 16 (2025) 56352. https://doi.org/10.1038/s41467-025-56352-5.

[14] Zhou, X., Fu, H., Shentu, B., Wang, W., Cai, S. and Bao, G., Design and control of a tendon-driven robotic finger based on grasping task analysis, Biomimetics, 9:6 (2024) 370. https://doi.org/10.3390/biomimetics9060370.

[15] Jiang, L., et al., Critical review on the relationship between design variables and performance of dexterous hands: a quantitative analysis, Frontiers in Neurorobotics, 19 (2025) 1513458. https://doi.org/10.3389/fnbot.2024.1513458.

[16] Park, J., Rhee, S., Kim, J., et al., Extension mechanism of the proximal interphalangeal joint of the human phalanx: a cadaveric biomechanical study, BioMed Research International, 2020 (2020) 2507239. https://doi.org/10.1155/2020/7585976.

[17] Engelhardt, L., Ferguson, S., Mylius, M., Henneman, M., van der Helm, F.C.T. and Veeger, D., A new musculoskeletal AnyBody™ detailed hand model, Computer Methods in Biomechanics and Biomedical Engineering, 24:16 (2021) 1780–1791. https://doi.org/10.1080/10255842.2020.1851367.

[18] McFarland, D.C., Binder-Markey, B.I., Nichols, J.A., Wohlman, S.J., de Bruin, M. and Murray, W\.M., A musculoskeletal model of the hand and wrist capable of simulating functional tasks, IEEE Transactions on Biomedical Engineering, 70:5 (2023) 1424–1435. https://doi.org/10.1109/TBME.2022.3217722.

[19] Park, H. and Kim, D., An open-source

anthropomorphic robot hand system: HRI hand, HardwareX, 7 (2020) e00100. https://doi.org/10.1016/j.ohx.2020.e00100.

[20] Tower Pro, MG90S Micro Servo datasheet, Tower Pro Servo Co. Ltd., (2015).